RANS Modeling in a Channel

Gopal Yalla, Clark Pederson, Tim Smith, Sean Carney

September 21, 2018

1 Developing the channel flow equations

We begin by developing the $k-\epsilon$ model for channel flow with Durbin's $\overline{v^2}-f$ formulation of the eddy viscosity near the wall. We chose this wall treatment since it fundamentally addresses the fact that near the wall, the eddy viscosity transports momentum in the vertical direction, and thus it should be a function of only the wall normal velocity fluctuations. The three-dimensional $\overline{v^2}-f$ model equations are given as:

$$\frac{\partial U_i}{\partial x_i} = 0 \tag{1}$$

$$\frac{\partial U_i}{\partial t} + U_j \frac{\partial U_i}{\partial x_j} = -\frac{\partial P}{\partial x_i} + \frac{\partial}{\partial x_j}\left(\nu \frac{\partial U_i}{\partial x_j} - r_{ij}\right) \tag{2}$$

$$\frac{\partial k}{\partial t} + U_j \frac{\partial k}{\partial x_j} = -r_{ij}\frac{\partial U_i}{\partial x_j} - \epsilon + \frac{\partial}{\partial x_j}\left(\frac{\nu_T}{\sigma_k}\frac{\partial k}{\partial x_j}\right) + \nu \frac{\partial^2 k}{\partial x_j \partial x_j} \tag{3}$$

$$\frac{\partial \epsilon}{\partial t} + U_j \frac{\partial \epsilon}{\partial x_j} = -\frac{1}{T}\left(C_{\epsilon 1}\mathcal{P} + C_{\epsilon 2}\epsilon\right) + \frac{\partial}{\partial x_j}\left(\frac{\nu_T}{\sigma_\epsilon}\frac{\partial \epsilon}{\partial x_j}\right) + \nu \frac{\partial^2 \epsilon}{\partial x_j \partial x_j} \tag{4}$$

$$\frac{\partial \overline{v^2}}{\partial t} + U_j \frac{\partial \overline{v^2}}{\partial x_j} = kf + \frac{\partial}{\partial x_j}\left((\nu_T + \nu)\frac{\partial \overline{v^2}}{\partial x_j}\right) - \epsilon \frac{\overline{v^2}}{k} \tag{5}$$

$$0 = f - L^2 \nabla^2 f - C_2 \frac{\mathcal{P}}{k} + \frac{C_1}{T}\left(\frac{\overline{v^2}}{k} - \frac{2}{3}\right) \tag{6}$$

where

$$r_{ij} = -\nu_T\left(\frac{\partial U_i}{\partial x_j} + \frac{\partial U_j}{\partial x_i}\right) + \frac{2k}{3}\delta_{ij}$$

$$\nu_T = \frac{3}{2} C_\mu \overline{v^2} T$$

$$\mathcal{P} = \nu_T\left(\frac{\partial U_j}{\partial x_i} + \frac{\partial U_i}{\partial x_j}\right)\frac{\partial U_j}{\partial x_i}$$

$$T = \max\left\{\frac{k}{\epsilon}, 6\left(\frac{\nu}{\epsilon}\right)^{\frac{1}{2}}\right\}$$

$$L = \max\left\{C_L \frac{k^{3/2}}{\epsilon}, C_\eta\left(\frac{\nu^3}{\epsilon}\right)^{1/4}\right\}$$

We consider channel flow through a rectangular duct of height $h = 2\delta$, with the bottom and top walls at $y = 0$ and $y = 2\delta$, and the midplane at $y = \delta$. In the fully developed case, the flow is steady and homogeneous in the streamwise and spanwise directions. Thus, statistics do not vary with time, or in the x and z direction. As in Pope [3] we neglect the mean spanwise velocity. We enforce the no slip condition at the boundary, so that $U_i = u_i = 0 \,\forall i$. Since at the wall $\frac{\partial U}{\partial x} = \frac{\partial W}{\partial z} = 0$, continuity implies that $\frac{\partial V}{\partial y} = 0$ and thus $V = 0$ everywhere. Moreover, the

flow is statistically symmetric about the mid-plane $y = \delta$. These assumptions and conditions imply that the original system, Eqns. (1)-(6), is simplified to:

$$-\frac{\partial P}{\partial x} + \frac{\partial}{\partial y}\left((\nu + \nu_T)\frac{\partial U}{\partial y}\right) = 0 \tag{7}$$

$$\nu_T\left(\frac{\partial U}{\partial y}\right)^2 + \frac{\partial}{\partial y}\left((\nu + \frac{\nu_T}{\sigma_k})\frac{\partial k}{\partial y}\right) = 0 \tag{8}$$

$$\frac{1}{T}\left(C_{\epsilon 1}\nu_T\left(\frac{\partial U}{\partial y}\right)^2 - C_{\epsilon 2}\epsilon\right) + \frac{\partial}{\partial y}\left((\nu + \frac{\nu_T}{\sigma_\epsilon})\frac{\partial \epsilon}{\partial y}\right) = 0 \tag{9}$$

$$kf - \frac{1}{T}\overline{v^2} + \frac{\partial}{\partial y}\left((\nu + \nu_T)\frac{\partial \overline{v}}{\partial y}\right) = 0 \tag{10}$$

$$L^2\frac{\partial^2 f}{\partial y^2} - f + C_2\frac{\nu_T}{k}\left(\frac{\partial U}{\partial y}\right)^2 - \frac{C_1}{T}\left(\frac{\overline{v^2}}{k} - \frac{2}{3}\right) = 0 \tag{11}$$

The constants are defined as follows:

1. $C_\mu = 0.19$
2. $C_k = 1.0$
3. $\sigma_\epsilon = 1.6$
4. $C_2 = 0.3$
5. $C_1 = 0.3$
6. $C_{\epsilon 1} = 1.55$
7. $C_{\epsilon 2} = 1.9$
8. $C_\eta = 70$
9. $C_L = 0.3$

1.1 Boundary conditions

For the turbulent channel, we only compute for $y \in [0, \delta]$, as opposed to the full $y \in [0, 2\delta]$, by symmetry. The boundary conditions for our five dependent variables, $U, k, \epsilon, \overline{v^2}, f$, are as follows:

$$U = k = \overline{v^2} = 0$$

at $y = 0$, which comes from the no-slip condition, which then implies

$$\epsilon \to 2\nu\frac{k}{y^2}, \quad f \to -\frac{20\nu^2\overline{v^2}}{\epsilon(0)y^4}$$

at $y = 0$. As a consequence of symmetry, we require homogeneous Neumann conditions on all of the dependent variables:

$$\frac{\partial U}{\partial y} = \frac{\partial \epsilon}{\partial y} = \frac{\partial \overline{v^2}}{\partial y} = \frac{\partial k}{\partial y} = \frac{\partial f}{\partial y} = 0$$

1.2 Nondimensionalization of the governing equations

Here we nondimensionalize (7)-(11) using the characteristic velocity scale u_τ (the friction velocity) and length scale δ. Abusing notation, we then make the following nondimensionalizations:

1. $U = U\big/u_\tau$
2. $\eta = y\big/\delta$
3. $t = t\big/(\delta/u_\tau), \quad T = T\big/(\delta/u_\tau)$
4. $\epsilon = \epsilon\big/(u_\tau^3/\delta)$

5. $\overline{v^2} = \overline{v^2}\Big/u_\tau^2$

6. $f = f\Big/(u_\tau/\delta)$

7. $\nu_T = \nu_T\Big/(u_\tau\delta)$

8. $L = L/\delta$

The above choice of units gives the following set of nondimensional equations for the $\overline{v^2} - f$ model as applied to fully developed channel flow:

$$\frac{\partial}{\partial\eta}\left(\left(\frac{1}{Re_\tau}+\nu_T\right)\frac{\partial U}{\partial\eta}\right) - 1 = 0 \tag{12}$$

$$\nu_T\left(\frac{\partial U}{\partial\eta}\right)^2 + \frac{\partial}{\partial\eta}\left(\left(\frac{1}{Re_\tau}+\frac{\nu_T}{\sigma_k}\right)\frac{\partial k}{\partial\eta}\right) = 0 \tag{13}$$

$$\frac{1}{T}\left(C_{\epsilon1}\nu_T\left(\frac{\partial U}{\partial\eta}\right)^2 - C_{\epsilon2}\epsilon\right) + \frac{\partial}{\partial\eta}\left(\left(\frac{1}{Re_\tau}+\frac{\nu_T}{\sigma_\epsilon}\right)\frac{\partial\epsilon}{\partial\eta}\right) = 0 \tag{14}$$

$$kf - \frac{1}{T}\overline{v^2} + \frac{\partial}{\partial\eta}\left(\left(\frac{1}{Re_\tau}+\nu_T\right)\frac{\partial\overline{v}}{\partial\eta}\right) = 0 \tag{15}$$

$$\left(L^2\frac{\partial^2}{\partial\eta^2} - I\right)f + C_2\frac{\nu_T}{k}\left(\frac{\partial U}{\partial\eta}\right)^2 - \frac{C_1}{T}\left(\frac{\overline{v^2}}{k} - \frac{2}{3}\right) = 0 \tag{16}$$

with this formulation, the boundary conditions are the same except for ϵ and f at the wall. These become:

$$\epsilon \to 2\frac{k}{Re_\tau y^2}, \quad f \to -\frac{20\overline{v^2}}{Re_\tau^2\epsilon(0)y^4}$$

at $y = 0$.

2 Discretization of the governing equations

2.1 Temporal Discretization and Time-Marching

As described in the previous section, we want to solve the steady state $\overline{v^2} - f$ equations for fully developed channel flow. We could try and do this by discretizing the steady equations and writing a nonlinear solver, but the equations are sensitive enough that the most naive solvers (e.g., Newton's method) will diverge unless one starts with a very accurate initial guess. One way around this problem is to use some sort of continuation method, often done by time marching. Essentially, we are looking to march in time from our initial guess to the steady state equations. Backward Euler is a good choice of time scheme because it is implicit (so one can take large steps) and because accuracy in time is not of importance. In fact, because we do not care about temporal accuracy, there is no need to fully solve the nonlinear system at each step,i.e., we can just take a single Newton iteration and go to the next step.

To be more specific, if $F(\xi) = 0$ is the system of equations given by (12)-(16), where, $\xi \equiv (U, k, \epsilon, \overline{v^2}, f)^T$, then we will start with an initial guess ξ_0 and solve $\partial\xi/\partial t = F(\xi)$, until $\partial\xi/\partial t \approx 0$. Generally, this works best by starting with a small time step and then gradually increasing the time step until it is very large. At this point we are essentially solving the steady problem from a different initial guess. Using a backward Euler scheme implies we are solving

$$\frac{\xi^{n+1} - \xi^n}{\Delta t} = F(\xi^{n+1}). \tag{17}$$

at each time step.

We will obtain our initial condition for $U, k, \epsilon, \overline{v^2}$ by interpolating DNS data from [1]. For f we were only able to get convergent results when we used an initial condition of all zeros. We

originally tried solving the elliptic equation for f given the initial interpolated results, however this always caused the time marching to diverge.

2.2 Spatial discretization

We choose to discretize our spatial derivatives with a centered differencing, so that

$$\frac{\partial \varphi}{\partial x} \approx \frac{\varphi_{i+1} - \varphi_{i-1}}{2\Delta x}$$

and

$$\frac{\partial^2 \varphi}{\partial x^2} \approx \frac{\varphi_{i+1} - 2\varphi_i + \varphi_{i-1}}{(\Delta x)^2}$$

for dummy dependent and independent variables φ and x, respectively. Note that these approximations hold for a uniform grid spacing Δx; the non-uniform grid case is detailed below. The fully discrete version of (17) then becomes

$$\frac{\xi_i^{n+1} - \xi_i^n}{\Delta t} = F_{\Delta\eta}(\xi_i^{n+1}) \implies G(\xi_i^{n+1}) = 0 \tag{18}$$

where $F_{\Delta\eta}$ is the discrete version of F and $G(\xi_i^{n+1}) \equiv \xi_i^{n+1} - \xi_i^n - \Delta t F_{\Delta\eta}(\xi_i^{n+1})$.

Given this setup, we march forward in time from ξ^0, performing one iteration of Newton's method per time step. Only one iteration is performed because we do not require temporal accuracy. Once $|\xi^{n+1} - \xi^n|$ is below some prescribed tolerance (here we chose 10^{-7}), we terminate our iterations and arrive at the approximate solution ξ^{n+1} such that

$$F_{\Delta\eta}(\xi^{n+1}) \approx 0.$$

3 Non-Uniform Grid

In order to reduce the computational requirements, a non-uniform spacing of points was used. This allows a fine resolution near the wall, where the resolution must be on the order of the wall-units, and a coarse resolution in the center of the channel. A set of uniform points, χ, was defined such that $\chi = 0$ corresponds to the channel wall and $\chi = 1$ corresponds to the centerline. This set of uniform points was remapped to the nonuniform mesh, $\eta = y/\delta$, using the mapping function used by Lee and Moser [1],

$$\eta = \frac{y}{\delta} = \frac{\sin(\lambda(\chi - 1)\pi/2)}{\sin(\lambda\pi/2)} + 1, \quad 0 \le \chi \le 1 \tag{19}$$

where λ is an adjustable parameter that controls the resolution near the wall. When λ is equal to 1, the wall-spacing is finest. When λ is very small, the mesh is approximately uniform. For our simulation, we use $\lambda = 0.97$. Using a value other than $\lambda = \pm 1$ prevents the derivative of y with respect to χ from going to zero at the walls.

The formula in Eq. 19 can be simplified by defining a few constants based on λ:

$$\eta = \frac{y}{\delta} = \frac{\sin\big((\chi - 1)a\big)}{b} + 1, \quad 0 \le \chi \le 1 \tag{20}$$

where $a = \lambda\pi/2$ and $b = \sin(\lambda\pi/2)$.

The inverse mapping and its derivatives can be written as:

$$\chi = \frac{\sin^{-1}(by - b)}{a} + 1 \tag{21}$$

$$\frac{\mathrm{d}\chi}{\mathrm{d}\eta} = \frac{b}{a\sqrt{1 - b^2(y-1)^2}} \tag{22}$$

$$\frac{\mathrm{d}^2\chi}{\mathrm{d}\eta^2} = \frac{b^2(by - b)}{a\big(1 - (b - by)^2\big)^{3/2}} \tag{23}$$

where a is a constant equal to the denominator in Eq. 19. Using the chain rule, the derivatives of a variable ϕ on the nonuniform grid, η can be computed using derivatives on the uniform grid, χ as follows:

$$\frac{\partial \phi}{\partial \eta} = \frac{\mathrm{d}\chi}{\mathrm{d}\eta}\frac{\partial \phi}{\partial \chi} \tag{24}$$

$$\frac{\partial^2 \phi}{\partial \eta^2} = \frac{\mathrm{d}^2\chi}{\mathrm{d}\eta^2}\frac{\partial \phi}{\partial \chi} + \left(\frac{\mathrm{d}\chi}{\mathrm{d}\eta}\right)^2 \frac{\partial^2 \phi}{\partial \chi^2} \tag{25}$$

In order to achieve a near-wall resolution on the order of $\Delta y\ \delta_v$, the distance between the first two grid points must be δ_v. This leads to the equation:

$$\Delta\chi = \frac{\sin^{-1}(b\delta_v - b)}{a} + 1 \tag{26}$$

If we use $\delta = 1$ as our channel width, then $y = \eta$ and $\delta_v = 1/\mathrm{Re}_\tau$. This leads to an equation for the required number of grid points, n, as:

$$n = \frac{a}{\sin^{-1}(b/Re_\tau - b) + a} \tag{27}$$

Using a value of $\lambda = .97$ for the mapping parameter, the number of points required for $\mathrm{Re}_\tau = 5200$ and $\mathrm{Re}_\tau = 10000$ is 390 and 735 respectively. This is significantly lower than the uniform grid sizes of 5,200 and 10,000.

4 Code Verification

We implemented a number of verification tests to make sure that our model was working as expected before computing results for $Re_\tau = 5,200$ and $10,000$. Notably, we ensured that the model converged to the laminar solution after setting $\nu_T \to 0$ and tested the model with $Re_\tau = 180$.

In the laminar case ($\nu_T = 0$), the mean velocity equations become,

$$\frac{1}{Re_\tau}\frac{\partial^2 U}{\partial \eta^2} + 1 = 0\ ,$$

which has an analytic solution of

$$U(y) = -\frac{Re_\tau}{2}\left(y^2 - 2y\right)\ .$$

This analytic solution and the computed velocity profile for the laminar case are shown in Fig. 1. Clearly the solution has converged to the analytic solution. Testing the laminar case verified our grid formulation, interpolation of DNS results for initial conditions, and that our numerical solver was working properly for the velocity equation, Eqn. (12).

Our next test was to compare our results from the $\overline{v^2} - f$ model with Durbin's results given in [4], for a $Re_\tau = 180$. This provided a more involved verification of the model. Durbin's $\overline{v^2} - f$ results are shown in Fig. 2 and ours are shown in Fig. 3. In each plot, the $\overline{v^2} - f$ results are compared with the corresponding DNS data. Our solution looks almost identical to Durbin's $\overline{v^2} - f$ results, and even disagrees with the DNS data in the same regions of the channel as Durbin. Our verified results at this stage gave us confidence that the model would behave well at high Reynolds numbers.

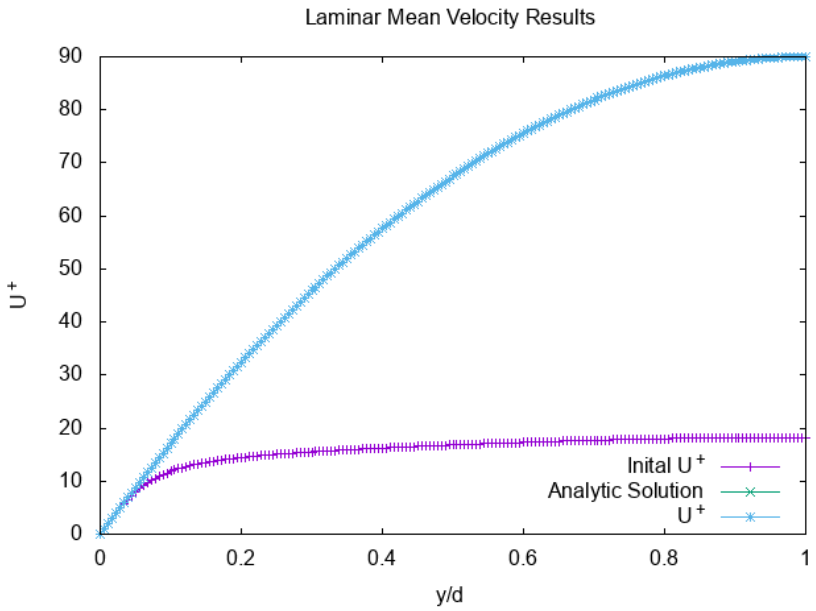

Figure 1: Laminar solution, Eqn. (12), computed with our $\overline{v^2} - f$ model. Note that our solution for U sits on top of the analytic solution.

5 Results for larger Re_τ

5.1 $Re_\tau = 5,200$ case

After verifying our code on the $Re_\tau = 180$ case, we ran our code at $Re_\tau = 5200$, so as to compare it with the DNS results of [1]. The results can be seen in Fig. 4.

Excellent agreement was found for the U profile. This is a testament to the strength of the $\overline{v^2} - f$ model, especially in the near-wall region. Good agreement was found for both the inner and outer layer, including the viscous sublayer.

The agreement were not as good for k or $\overline{v^2}$. This matches what was seen for $Re_\tau = 180$ in Durbin's paper [4], as discussed in the previous section. The lack of agreement also reflects the nature of the $\overline{v^2} - f$ model, where U is usually the quantity of interest, whose model is built upon parameters k, ϵ, $\overline{v^2}$ and f. Due to the differences between reality and the model for U, the parameters such as k do not have to be precise to give the correct behavior for U. Nevertheless, the overall behavior of k and $\overline{v^2}$ is still close to the DNS data.

Similarly, a comparison of the RANS results for ε with the DNS data shows slight difference, especially near the wall. Nevertheless, the overall behavior is still close to the DNS data.

5.2 $Re_\tau = 10000$ case

Results for the $Re_\tau = 10000$ case are shown in Fig. 5. Also shown in this figure are the results for $Re_\tau = 5200$. The U and ε profiles are almost exactly the same when normalized by y^+ units, with a slightly longer log-law region at the higher Reynolds number. In Fig. 6 we show the mean velocity profiles given by the $\overline{v^2} - f$ equation for $Re_\tau = 180, 2000, 5200$, and $10,000$.

5.3 Log-Law Parameters

The RANS results for the $Re_\tau = 5200$ case were also compared to the log-law. The "universal values" given by Pope [3] did not fit as well as the values derived from DNS by Lee and Moser [1]. These values are $\kappa = 0.384$ and $B = 4.27$. A comparison of the RANS results with the theoretical log-law is shown in Fig. 7. This agreement with the values put forth by Lee and

Moser is logical, since the RANS U profile closely matches the DNS results. For the $Re_\tau = 10000$ case, a linear-log regression was used to fit the log-law to the data between $y^+ = 30$ and $\eta < 0.3$. In this region, we obtained values of $\kappa = 0.378$ and $B = 4.013$, with a correlation coefficient of $r = 0.999$. These are slightly lower than the previous values, but the fit is still very good in the log-law region, as shown in Fig. 8.

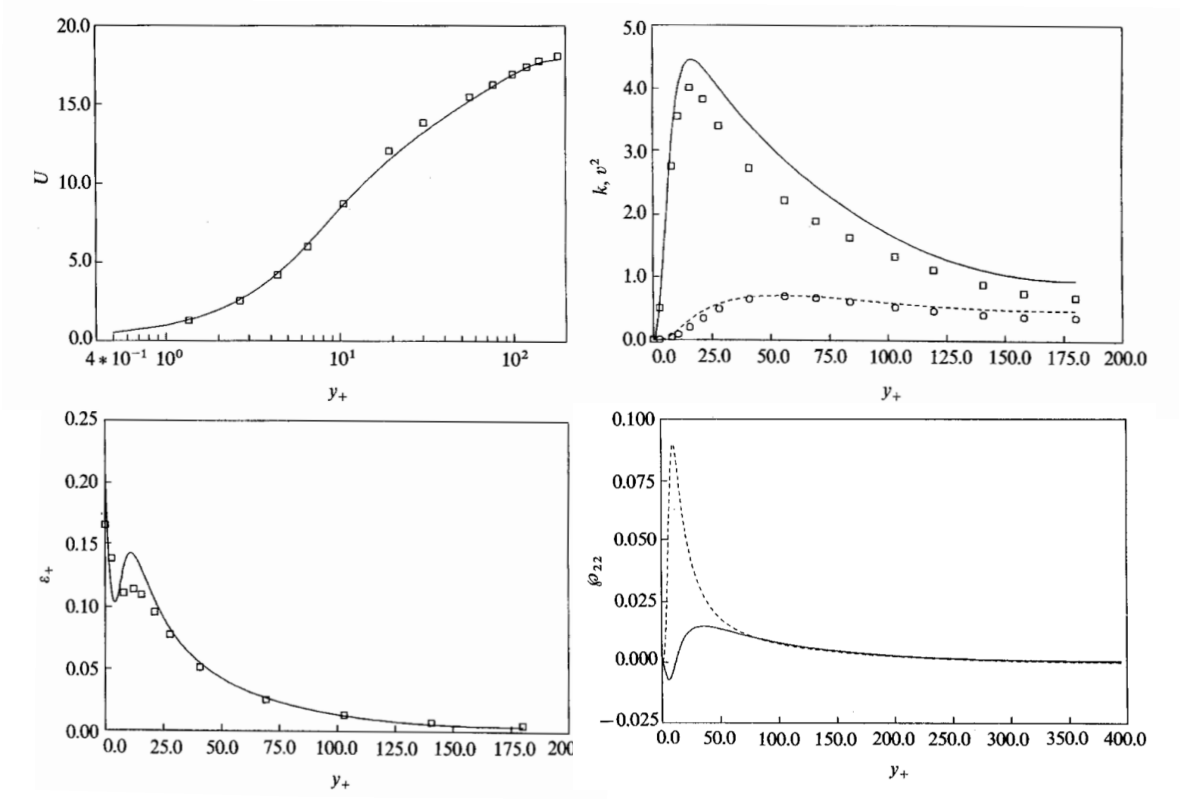

Figure 2: Steady solutions for channel flow at $Re_\tau = 180$ from DNS (circles) and the $\overline{v^2} - f$ model (lines) taken from [4]. Each plot is as labeled, and the solid black line on the bottom right figure shows kf. Note that the bottom right plot only is generated from simulations at $Re_\tau = 395$ but we include it here because it gave us intuition for how f should behave while verifying our model.

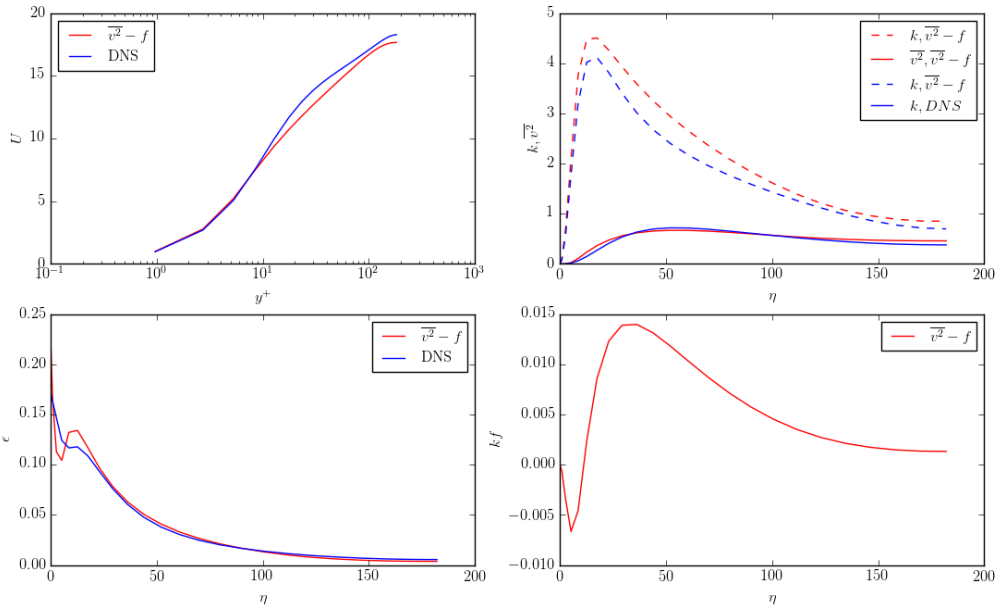

Figure 3: Steady state solution to the $\overline{v^2} - f$ model, Eqns. (12)-(16), at $Re_\tau = 180$. The red lines show results from our model while the blue lines show our initial conditions which are interpolated DNS results from [1]. Note we show no initial data for kf since f is initialized at zero.

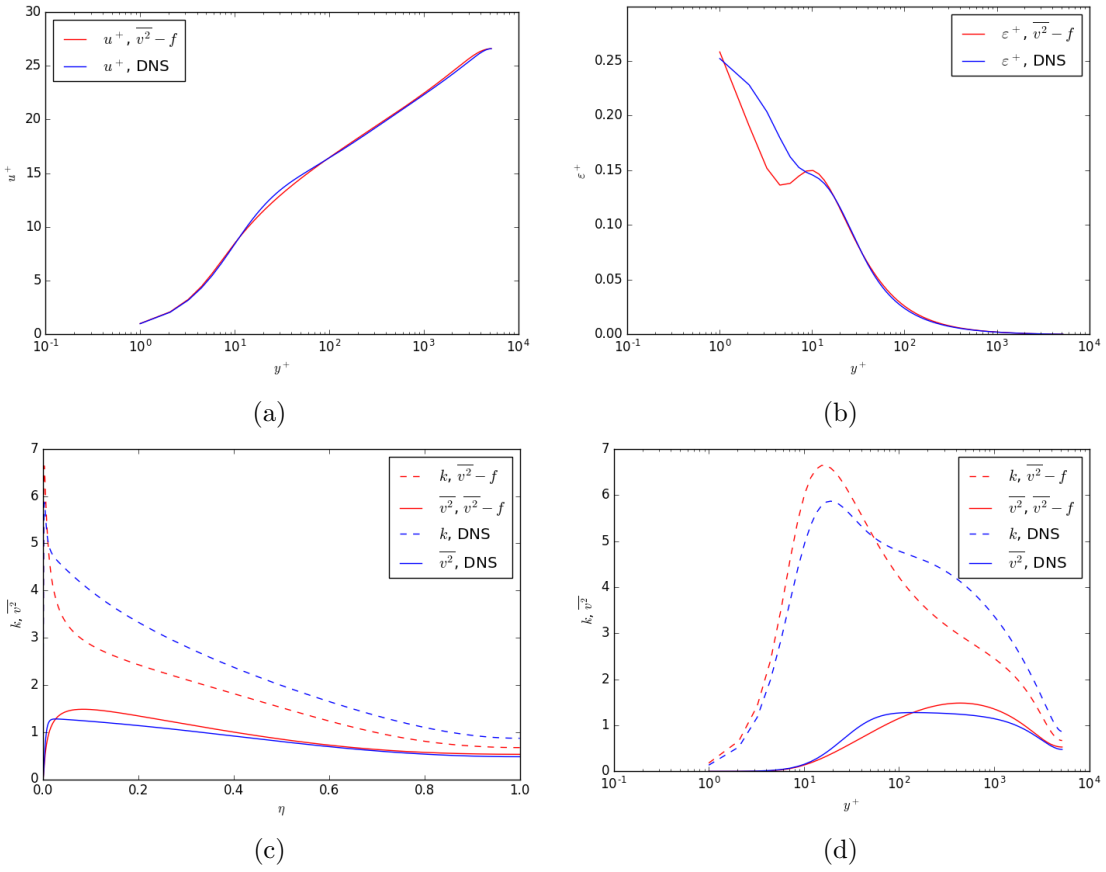

Figure 4: Steady state solutions for $Re_\tau = 5200$. (a) The mean velocity, U. (b) The dissipation, ε^+, normalized in wall-units. (c) The turbulent kinetic energy, k, and the wall-normal velocity variance, $\overline{v^2}$, normalized by the channel width. (d) k and $\overline{v^2}$, normalized by wall-units

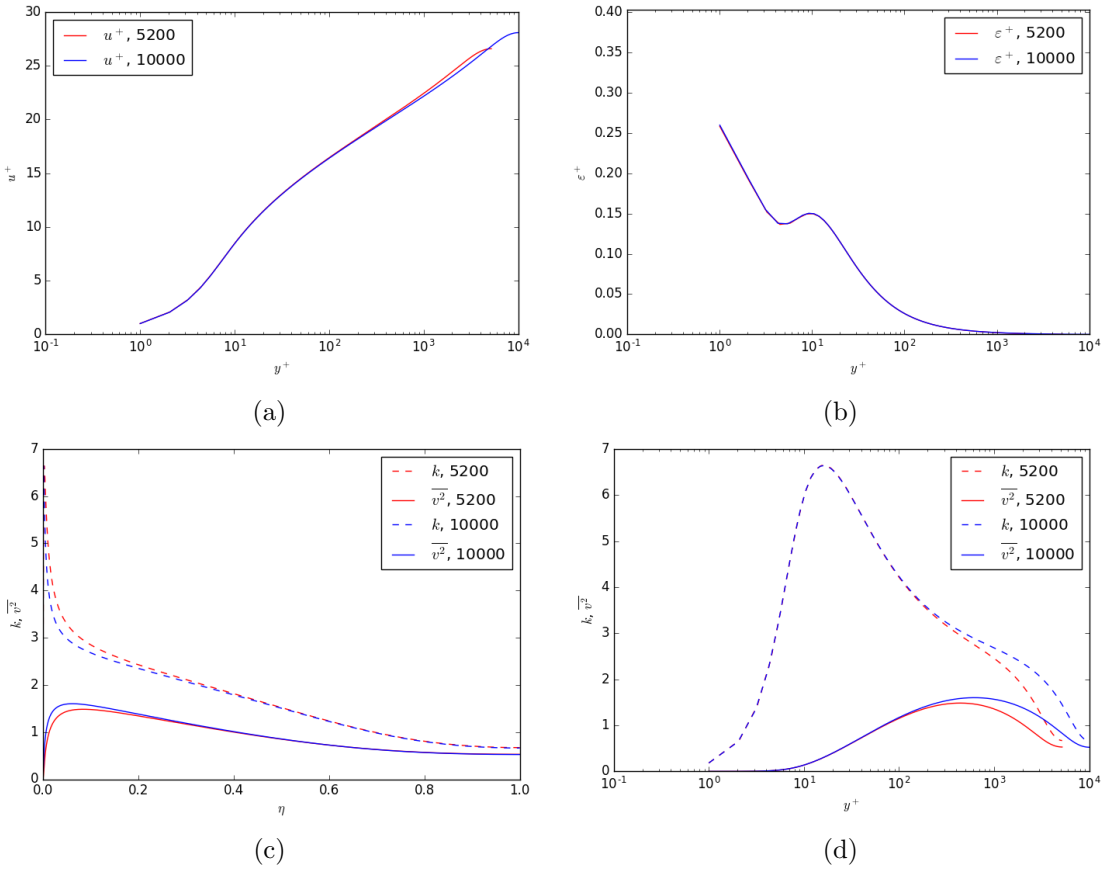

Figure 5: A comparison of steady state solutions for $Re_\tau = 5200$ and $Re_\tau = 10000$. (a) The mean velocity, U. (b) The dissipation, ε^+, normalized in wall-units. (c) The turbulent kinetic energy, k, and the wall-normal velocity variance, $\overline{v^2}$, normalized by the channel width. (d) k and $\overline{v^2}$, normalized by wall-units

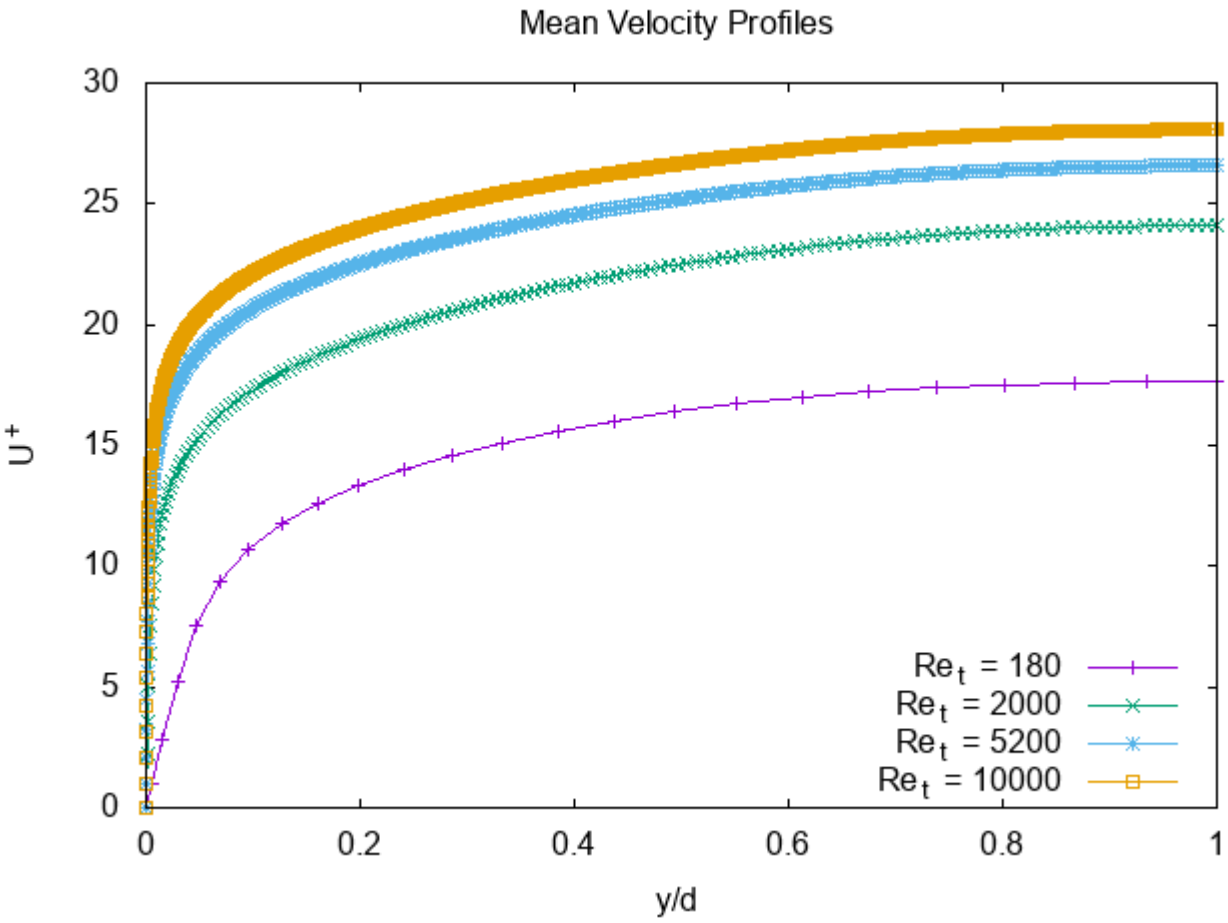

Figure 6: Results from the $\overline{v^2} - f$ model at $Re_\tau = 180, 2000, 5200, 10000$.

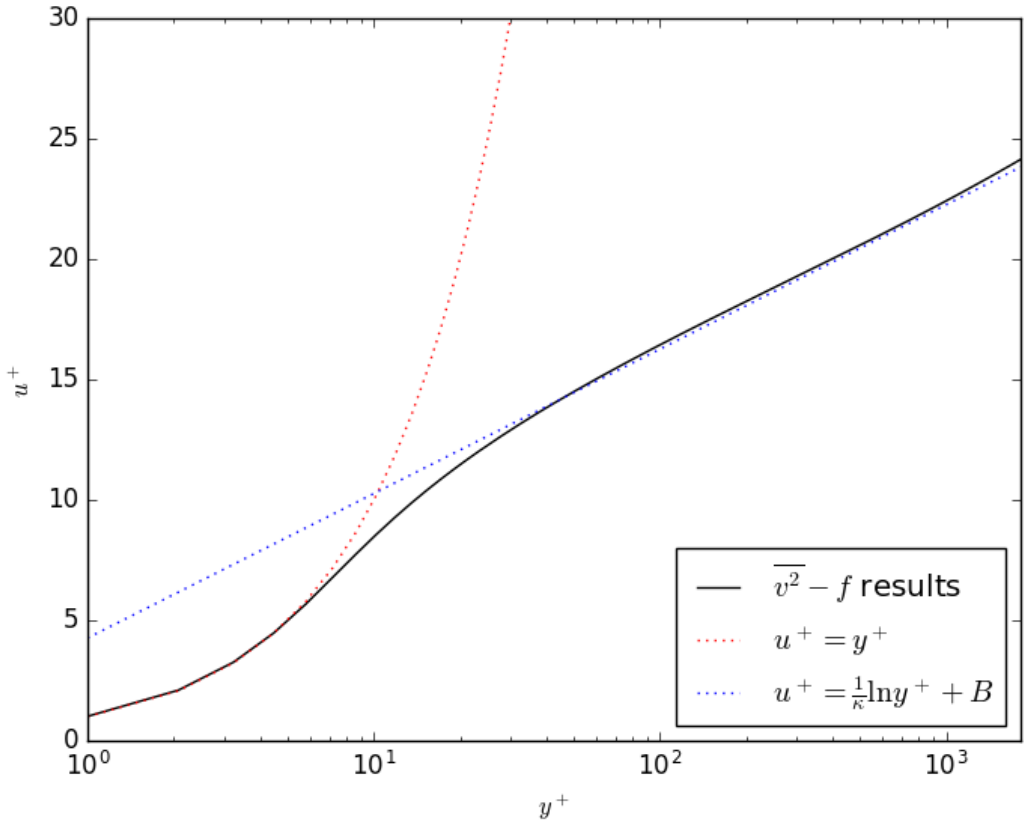

Figure 7: Comparison of the $Re_\tau = 5200$ results with the expected power-law and log-law behavior near the wall. The values of $\kappa = 0.384$ and $B = 4.27$ give good agreement between the log-law and the RANS results.

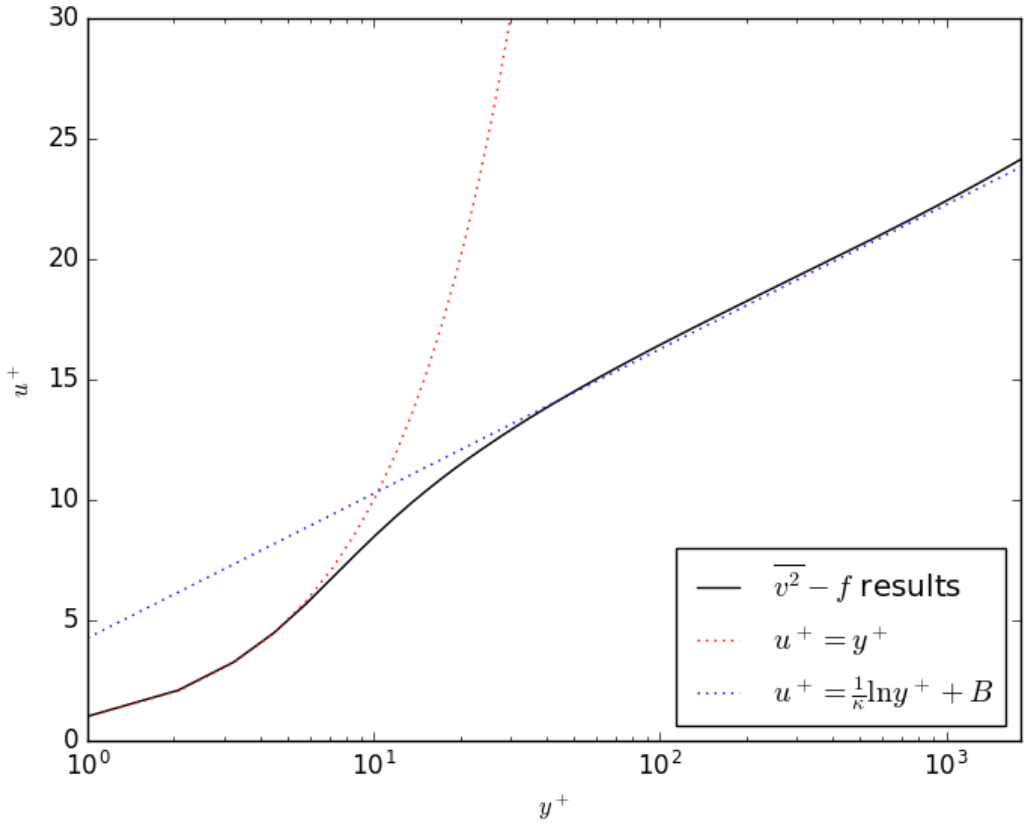

Figure 8: Comparison of the $Re_\tau = 10000$ results with the expected power-law and log-law behavior near the wall. The values of $\kappa = 0.378$ and $B = 4.013$ give good agreement between the log-law and the RANS results.

References

[1] Lee, Myoungkyu and R.D. Moser, "Direct numerical simulation of turbulent channel flow up to $Re_\tau = 5200$," J. Fluid Mech. 774 (2015) 395415. doi:10.1017/jfm.2015.268.

[2] Durbin, Paul A., and BA Pettersson Reif. *Statistical theory and modeling for turbulent flows.* John Wiley & Sons, 2011.

[3] Pope, Stephen B. *Turbulent flows.* (2001): 2020.

[4] Durbin, Paul A. "Near-wall turbulence closure modeling without damping functions." Theoretical and Computational Fluid Dynamics 3.1 (1991): 1-13.